PAPER

Effect of the aromatic substituent on the *para*-position of pyridine-bis(oxazoline) sensitizers on the emission efficiency of their Eu[III] and Tb[III] complexes†

Ana de Bettencourt-Dias, [ID] * Jeffrey S. K. Rossini and Josiane A. Sobrinho

Two efficient lanthanide ion sensitizers 2,6-bis(oxazoline)-4-phenyl-pyridine (PyboxPh, **1**) and 2,6-bis(oxazoline)-4-thiophen-2-yl-pyridine (Pybox2Th, **2**) were synthesized. **1** crystallizes in the monoclinic space group $P21/c$ with cell parameters a = 16.3794(4) Å, b = 7.2856(2) Å, c = 11.7073(3) Å, β = 97.229(1)° and V = 1385.97(6) Å³. **2** crystallizes in the monoclinic space group $P21/n$ with cell parameters a = 5.9472(2) Å, b = 16.0747(6), c = 14.3716(5) Å, β = 93.503(1)° and V = 1371.35(8) Å³. Photophysical characterization of **1** shows that its triplet state energy is located at 22 250 cm⁻¹ and efficient energy transfer is observed for Eu[III] and Tb[III]. Solutions of [Ln(PyboxPh)₃]³⁺ in dichloromethane display an emission efficiency of 37.2% for Ln═Eu and 24.0% for Ln═Tb. The excited state lifetimes for Eu[III] and Tb[III] are 2.227 ms and 723 μs, respectively. The triplet state energy of **2** is located at 19 280 cm⁻¹ and is therefore too low to efficiently sensitize Tb[III] emission. However, the sensitization of Eu[III] is effective, with an emission quantum yield of 14.5% and an excited state lifetime of 714 μs. This shows that the derivatization of the chelator is strongly influenced by the aromatic substituents on the *para*-position of the pyridine ring. New isostructural 1 : 1 complexes of PyboxPh with Eu[III] (**3**) and Tb[III] (**4**) were also isolated and crystallize in the triclinic space group $P\bar{1}$ with cell parameters a = 9.1845(2) Å, b = 10.3327(2) Å, c = 11.9654(2) Å, α = 98.419(1)°, β = 108.109(1)°, γ = 91.791(1)°, V = 1064.08(4) Å³ and a = 7.8052(1) Å, b = 11.8910(1) Å, c = 14.2668(2) Å, α = 72.557(1)°, β = 86.355(1)°, γ = 77.223(1)°, V = 1231.95(3) Å³, respectively.

Introduction

Lanthanide (Ln[III]) ions are known as highly efficient light emitters *via* metal-centred f–f transitions. The long lived excited states give rise to narrow emission bands,[1–3] making these complexes desirable phosphors for a myriad of applications such as displays, fluoroimmuno-assays, biosensors and protein tagging.[4,5] Since direct metal-centred excitation is inefficient, due to the parity-forbidden nature of the electric dipole f–f transitions, efficient population of the f-excited states is achieved through coordinated ligands, in which successive population of the ligands' singlet and triplet states through absorption and intersystem crossing and subsequent energy transfer to the metal center results in characteristic Ln[III] ion luminescence.[1–3] This process is commonly referred to as the antenna effect and has been extensively studied by

others[1,6–37] as well as by our research group.[38–52] Pyridine-2,6-bis(oxazoline) (Pybox) has garnered large attention as a ligand in transition metal complexes for asymmetric catalysis,[53] and several examples are known in which the transition metal is replaced by a rare earth.[53–55] More recently, we[56–58] and others[59] demonstrated its use as a sensitizer. We evaluated the sensitizing efficiency of a Pybox antenna derivatized with thiophen-3-yl at the *para* position of the pyridine ring (Pybox3Th).[56] This ligand yielded complexes of Eu[III] and Tb[III] with emission quantum yields of 76 and 59%, respectively. The triplet state of Pybox3Th is located at 21 080 cm⁻¹. By comparison, Pybox with non-aromatic groups, such as H, Br and OAlkyl at the *para* position of the pyridine, have triplet state energies in the range 23 260–26 700 cm⁻¹ and display luminescence quantum yields in the 20–30% range for both metal ions.[60] We therefore attributed the favourable position of the excited state to the resonance effect of the thiophene moiety. To further probe the relationship between the aromatic nature of the substituent at the *para* position of the Pybox pyridine ring and its effect on the singlet and triplet state energy levels, we targeted additional ligands with different aromatic moieties on this position. Several groups have studied the effect of tar-

Department of Chemistry, University of Nevada, Reno, NV 89557, USA.
E-mail: abd@unr.edu; Fax: +1775 784 6804; Tel: +1 775 682 8421
†Electronic supplementary information (ESI) available. CCDC 890798 for **3**, 890799 for **2**, 890800 for **1** and 890801 for **4**. For ESI and crystallographic data in CIF or other electronic format see DOI: 10.1039/d0dt03135f

geted substitution of aromatic rings with electron-withdrawing and electron-donating groups, which alter the electronic energy levels of the ligands, to optimize the efficiency of inter-system crossing and of energy transfer from the ligands' triplet state to the emissive state of the Ln[III] ion.[61–66] The effect of the substituents on the triplet and singlet states of the ligands seems to depend on the type of ligand family observed. Fewer studies were undertaken with systematic changes in aromaticity of the ligands,[67–70] some of which conclude that more extended conjugation leads to lower energy levels, as would be expected, while in other cases no direct effect of the substituents on the energy levels of the ligands is observed and other parameters, such as the metal ion's coordination environment, are invoked instead to explain differences in emission efficiency.[71] Our previous work demonstrates that the triplet state of a Pybox with an extended aromatic system is substantially lower than the triplet states of the other Pybox ligands, as mentioned above. We have explored two more aromatic substituents and their effects on the singlet and triplet energy levels of the sensitizers, and report here the synthesis of the two antennas, 2,6-bis(oxazoline)-4-phenyl-pyridine (PyboxPh, **1**)[72] and the new 2,6-bis-(4,5-dihydro-oxazol-2-yl)-4-thiophen-2-yl-pyridine (Pybox2Th, **2**). Complete photophysical characterization of these compounds shows the successful manipulation of the singlet and triplet state energy levels. Comparison of the photophysical properties of the new sensitizers **1** and **2** to that of the previously published Pybox3Th supports our initial assumption that substitution of the thiophen-3-yl functional group with other aromatic groups greatly influences the ligands' excited triplet state, tuning it to levels close to the emissive states of Eu[III] and Tb[III], leading therefore to high emission quantum yields. While this is straightforward in the case of **1**, the triplet state of **2** was altered in such a way as to efficiently sensitize the emission of Eu[III], but too low in energy to sensitize Tb[III] emission. The structures of both ligands and of the 1:1 complexes of PyboxPh with Eu[III] and Tb[III] are discussed here as well.

Experimental section

All commercially obtained reagents were of analytical grade and used as received. Solvents were dried by standard methods. Unless otherwise indicated, all syntheses were performed under N_2. Ln[III] salts were dried under reduced pressure and heating to 100 °C overnight and kept in a glove box under controlled atmosphere (O_2 < 0.5 ppm, H_2O < 1.0 ppm). The final lanthanide ion concentration was determined through titration with EDTA the presence of xylenol orange as the indicator.[73] Samples were prepared by diluting solutions to 1×10^{-4} M in acetonitrile in a glove box. Unless otherwise indicated, all data were collected at a constant temperature of 25.0 ± 0.1 °C. NMR spectra were recorded on Varian 400 or 500 MHz spectrometers with chemical shifts (δ, ppm) reported against tetramethylsilane (TMS). Electrospray ionization mass spectra (ESI-MS) were collected in positive ion mode on a

Waters Micromass ZQ quadrupole mass spectrometer. All samples were filtered through a 0.2 μm syringe filter before injecting into the mass spectrometer.

4-Bromo-2,6-bis-(4,5-dihydro-oxazol-2-yl)-pyridine (PyboxBr) was synthesized as previously reported.[60]

Synthesis of 2,6-bis(oxazoline)-4-phenyl-pyridine, PyboxPh (1)

1.83 g (6.20 mmol) of 4-bromo-2,6-bis-(4,5-dihydro-oxazol-2-yl)-pyridine, 0.84 g (6.87 mmol) of benzeneboronic acid, 1.74 g (13.77 mmol) of K_2CO_3 and 0.16 g (0.14 mmol) of tetrakis(triphenylphospine)palladium(0) were dissolved in 150 ml of THF and refluxed for 24 h. The resulting crude product was diluted with $CHCl_3$ (50 ml) and washed with water (3 × 10 ml) and brine (3 × 10 ml). The organic layer was dried over $MgSO_4$ and the solvent removed to give a light brown residue. The crude material was further purified by flash chromatography on alumina (99.5% $CHCl_3$: 0.5% MeOH) to give 1.31 g (4.48 mmol) of PyboxPh as a white powder. Yield = 72.3%. ^{1}H-NMR (400 MHz, $CDCl_3$) δ 8.43 (s, 2H), 7.77 (m, 2H), 7.48 (m, 3H), 4.57 (t, J = 12 Hz, 4H), 4.15 (t. J = 12 Hz, 4H). ESI-MS [M + H]$^+$ (experimental) 294.29 m/z (calculated) 294.33 m/z. MS [M + Na]$^+$ (experimental) 316.21 m/z (calculated) 316.31 m/z.

Synthesis of 2,6-bis-(4,5-dihydro-oxazol-2-yl)-4-thiophen-2-yl-pyridine, Pybox2Th (2)

1.75 g (5.91 mmol) of 4-bromo-2,6-bis-(4,5-dihydro-oxazol-2-yl)-pyridine, 0.84 g (6.54 mmol) of 2-thiopheneboronic acid, 1.81 g (13.07 mmol) of K_2CO_3 and 0.15 g (0.13 mmol) of tetrakis(triphenylphosphine)palladium(0) were dissolved in 150 ml of THF and refluxed for 24 h. The resulting crude product was diluted with $CHCl_3$ (50 ml) and washed with water (3 × 10 ml) and brine (3 × 10 ml). The organic layer was dried over $MgSO_4$ and the solvent removed under reduced pressure to give a light grey residue. The crude material was further rinsed with a 5:1 solution of ethyl acetate : petroleum ether. The remaining solid was dried under reduced pressure to give 0.26 g (0.87 mmol) of Pybox2Th. Yield = 60.0% ^{1}H NMR (400 MHz, $CDCl_3$) 8.36 (s, 2H), 7.66 (m, 1H), 7.48 (m, 1H), 7.16 (m, 1H), 4.56 (t, J = 12 Hz, 4H), 4.15 (t, J = 12 Hz, 4H). ESI-MS [M + H]$^+$ (experimental) 300.37 m/z (calculated) 300.36 m/z.

Synthesis of metal complexes

The metal complexes with 1:1 stoichiometry were prepared in air by mixing 1:1 amounts of 1×10^{-4} M chloroform solution of ligand and 1×10^{-4} M acetonitrile solution of Ln(NO$_3$)$_3$ (Ln = La, Eu, Tb), and stirred for a minimum of 1 hour at room temperature. The solutions were filtered and vapor diffusion of n-pentane into THF/acetonitrile solutions yielded X-ray quality crystals within a week. Because only crystallization was attempted and bulk solids where not routinely isolated from the solution, yields were not determined. Photophysical characterization was performed on solutions of 3:1 complexes of Eu[III] and Tb[III] as the triflate salts in dichloromethane (1×10^{-4} M), the stoichiometry which ensures saturation of the coordination sphere with ligands. The 3:1 stoichiometry of

the Eu^{III} and Tb^{III} complexes was confirmed by absorption titrations (Fig. S3–S6†).

X-ray crystallographic characterization

Crystal data, data collection, and refinement details for compounds **1–4** are given in Table 1. Suitable crystals were mounted on a glass fiber and placed in a low temperature nitrogen stream. Data were collected on a Bruker SMART CCD area detector diffractometer equipped with a low-temperature device, using graphite-monochromated Mo-Kα radiation (λ = 0.71073 Å). Data were measured using a strategy combining ω and φ scan frames of 0.3° per frame and an acquisition of 10 or 20 s per frame. Multi-scan absorption corrections were applied. Cell parameters were retrieved using SMART[74] software and refined using SAINTPlus[75] software on all observed reflections. Data reduction and correction for Lp and decay were performed using the SAINTPlus[75] software. Absorption correction was applied using SADABS.[76] The structures were solved by direct methods and refined by least-square methods on F^2 using the SHELXTL[77] programming package. All non-hydrogen atoms were refined anisotropically. The hydrogen atoms were added geometrically and their parameters constrained to the parent site. For complexes with coordinated water molecules and water molecules of crystallization, hydrogen atoms could not be located on the difference map, could not be added geometrically, and have been omitted, although the formulas are correct. CCDC 890800 corresponds to the structure of **1**, CCDC 890799 for **2**, CCDC 890798 for **3** and CCDC 890801 for **4**.†

Photophysical characterization

Solutions for spectroscopic studies were prepared by mixing the ligands with lanthanide triflates in acetonitrile in 3 : 1 stoichiometry in a glovebox with controlled atmosphere (O_2 <

0.5 ppm, H_2O < 1.0 ppm). The solutions were diluted to the concentration indicated in the captions and allowed to equilibrate overnight prior to measurement. Absorption spectra were measured on a PerkinElmer Lambda 35 spectrometer. For the absorption titrations, the spectra were collected in a Shimadzu UV-2550 UV-Vis spectrophotometer. The stoichiometry was determined through absorption titration of the ligands (1 × 10^{-4} M, dichloromethane) with aliquots of $Ln(CF_3SO_3)_3$ (Ln = Eu^{III} or Tb^{III}) (1 × 10^{-3} M, acetonitrile) at 25 °C. The solution was adjusted to a final concentration of 5 × 10^{-5} M with respect to the ligand in 1 : 1 dichloromethane : acetonitrile and stirred to equilibrate for 24 h before measuring. These experiments were performed in duplicate.

Emission spectra were measured on a PerkinElmer LS-55 fluorescence spectrometer or on a Horiba Jobin Yvon Fluorolog 3 spectrometer. Slit widths for emission and excitation measurements were 5 and/or 10 nm and a scan rate of 250 nm s^{-1} was used. On the PerkinElmer, the data were collected in phosphorescence mode with an initial delay of 0 ms, a cycle time of 16 ms and a gate time of 0.5 ms and filters to cut off the wavelengths of the excitation beam as appropriate. Excitation and emission spectra were corrected for instrumental function.

For quantum yield measurements, the absorption and emission/excitation spectra were measured using 0.2 cm path length cells, making sure that the spectra were at a right angle configuration to the excitation light and along the long path length (1 cm). Quantum yields were calculated using the equation below.

$$\Phi_x = \frac{n_x{}^2 A_{\text{ref}} I_{\text{ref}} E_x}{n_{\text{ref}}{}^2 A_x I_x E_{\text{ref}}} \times \Phi_{\text{ref}} \qquad (1)$$

Φ is the quantum yield of sample x and reference ref, n is the refractive index (1.343 in acetonitrile, 1.33287 in water), A the

Table 1 Details of the X-ray crystallographic characterization of compounds **1–4**

Compound	PyboxPh	Pybox2Th	[Eu(PyboxPh)(NO₃)₃H₂O]	[Tb(PyboxPh)(NO₃)₃H₂O]·2H₂O
CCDC number	890800†	890799†	890798†	890801†
Formula	$C_{17}H_{15}N_3O_2$	$C_{15}H_{13}N_3O_2S$	$C_{17}H_{17}N_6O_{12}Eu$	$C_{17}H_{19}N_6O_{14}Tb$
M/g mol^{-1}	293.32	299.35	649.32	690.30
Crystal system	Monoclinic	Monoclinic	Triclinic	Triclinic
Space group	$P2_1/c$	$P2_1/n$	$P\bar{1}$	$P\bar{1}$
a/Å	16.379(4)	5.947(2)	9.184(5)	7.805(2)
b/Å	7.285(6)	16.074(8)	10.332(7)	11.891(0)
c/Å	11.707(3)	14.371(7)	11.965(4)	14.266(8)
α/°	90	90	98.41(9)	72.55(7)
β/°	97.23(0)	93.50(3)	108.10(9)	86.35(5)
γ/°	90	90	91.79(1)	77.23(3)
V/Å^3	1385.9(76)	1371.3(58)	1064.0(8)	1231.9(53)
T/K	100(2)	100(2)	100(2)	100(2)
Z	4	4	2	2
D_c/g cm^{-3}	1.406	1.461	1.976	1.874
μ(Mo-Kα)/mm^{-1}	0.7107	0.7107	0.07107	0.07107
Independent reflections, R_{int} [$F_o \geq 4\sigma(F_o)$]	5286, 0.0321	4006, 0.0347	3740, 0.0363	6904, 0.0417
Reflections collected	27 021	27 642	17 708	33 249
Date/restraints/parameters	5286/0/259	4006/0/185	3740/0/319	6904/12/349
Goodness-of-fit on F^2	2.944	1.043	1.032	1.085
R_1, wR_2 (all data)	0.0838, 0.0929	0.0679, 0.1509	0.0240, 0.0531	0.0459, 0.0955
Largest diff. peak and hole/e Å$^-$	0.775, −0.488	0.890, −0.496	1.208, −0.480	2.826, −2.282

absorbance at the excitation wavelength, I the intensity of the corrected excitation spectrum at the excitation wavelength and E the integrated corrected emission spectrum. The spectra are corrected for instrumental function. The references were $Cs_3[Eu(dipic)_3]$ (Φ_{ref} = 24.0%. A_{279} ~ 0.05, 6.5×10^{-5} M) and $Cs_3[Tb(dipic)_3]$ (Φ_{ref} = 22.0%. A_{279} ~ 0.05, 6.5×10^{-5} M) in tris buffer (0.1 M).[78,79] Triplet and singlet state measurements were performed at 77 K with solutions of the same stoichiometry and using Gd^{III} as the metal ion[9] and are indicated as the 0–0 transition, after deconvolution of the fluorescence and phosphorescence spectra into their Franck–Condon progression.

The intrinsic quantum yield ϕ_{Eu}^{Eu} was determined from the excited state emissive lifetime τ_{exp} using eqn (2)[80]

$$\phi_{Eu}^{Eu} = \frac{\tau_{exp}}{\tau_R} \qquad (2)$$

and the radiative lifetime τ_R is given by eqn (3).[80]

$$\frac{1}{\tau_R} = A(^5D_0 \rightarrow {}^7F_1)n^3 \left(\frac{E(^5D_0 \rightarrow {}^7F_J)}{E(^5D_0 \rightarrow {}^7F_1)} \right) \qquad (3)$$

In this equation, $A(^5D_0 \rightarrow {}^7F_1)$ is the spontaneous emission probably of the magnetic dipole allowed transition $^5D_0 \rightarrow {}^7F_1$ (14.65 s^{-1} in vacuum), n is the refractive index of the medium, and E are the integrated emission areas of the whole spectrum $^5D_0 \rightarrow {}^7F_J$ (J = 0–6) and of the magnetic dipole allowed transition $^5D_0 \rightarrow {}^7F_1$. The sensitization efficiency (η_{sens}) was determined using eqn (4).

$$\eta_{sens} = \frac{\Phi_x}{\phi_{Eu}^{Eu}} \qquad (4)$$

Calculations

Calculations were performed with the help of the graphical user interface Lumpac.[81] The geometries of the 3 : 1 and 1 : 1 complexes, using the initial geometries from the 1 : 1 experimentally determined crystal structures, were optimized with Mopac2012 at the PM7 level of theory,[82] using a+3 Sparkle to model the metal ions.[81] The singlet and triplet state energies were estimated by TD-DFT using Orca,[83] modeling the metal ions as point charges, as CIS calculations, implemented under Lumpac,[81] significantly underestimated the excited state energies.

Results and discussion

Two new sensitizers for Ln^{III} ion luminescence based on *para*-derivatized pyridine-bis(oxazoline), namely phenyl-derivatized Pybox (PyboxPh, **1**) and thiophen-2-yl-derivatized Pybox (Pybox2Th, **2**) were synthesized and characterized by standard methods. Their solutions with Eu^{III} and Tb^{III} are luminescent and the emission efficiency was quantified for the 3 : 1 solution stoichiometry. X-ray quality crystals of 1 : 1 complexes of Eu^{III} and Tb^{III} with the PyboxPh ligand were isolated. When examined under the light of a hand-held UV lamp (λ =

245 nm), the crystals display the characteristic red or green luminescence of the corresponding Ln^{III} ion.

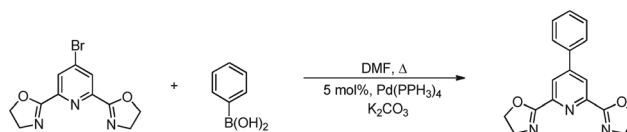**Synthesis and characterization of PyboxPh (1) and Pybox2Th (2)**

PyboxPh, **1**, was obtained in 72% overall yield, after purification by flash chromatography, by reacting PyboxBr with phenyl-boronic acid under Suzuki coupling conditions, as shown in Scheme 1.

X-ray quality crystals of **1** were obtained after vapor diffusion of *n*-pentane in THF/MeCN. Its structure is shown in Fig. 1 and details of all crystallographic characterizations are summarized in Table 1. **1** crystallizes in the monoclinic $P2_1/c$ space and displays a relatively planar configuration, with dihedral angles of 25.9(4)° between the phenyl and pyridine rings, and 19.0(3)° and 1.3(5)° between the oxazoline and pyridine rings. Four molecules are present in the unit cell of **1**, as shown in Fig. 2. The packing is dominated by π–π stacking interactions between the phenyl rings (Fig. 3), with a distance between the ring centroids of 3.76(6) Å and an interplanar distance of 3.44(7) Å, both typical of π–π interactions.[84]

As shown in Fig. 4, in acetonitrile, **1** absorbs at 208 nm and, upon excitation at 340 nm, it emits at 403 nm.

Pybox2Th, **2**, was obtained in an overall yield of 60% by reacting PyboxBr with thiophen-2-yl-boronic acid under Suzuki coupling conditions, as shown in Scheme 2. The crude material was purified by rinsing with a 5 : 1 solution of ethyl acetate and petroleum ether.

X-ray quality crystals of **2** could be obtained after vapor diffusion of *n*-pentane in THF/MeCN. Its structure is shown in Fig. 5 and details of the crystallographic characterization are summarized in Table 1. **2** crystallizes in the monoclinic space group $P2_1/n$ with four molecules in the unit cell. The ligand displays an almost planar configuration, with dihedral angles of 12.9(4)° between the thiophene and pyridine rings, and 5.4(1)° and 5.5(4)° between the oxazoline and pyridine rings. The thiophene ring is disordered, as is often seen in compounds bearing this functional group,[85] with two possible orientations which are rotated by 180° along the C3–C4A bond. The major component refined to 54.0% occupancy. The packing structure (Fig. 6) shows a wave-like structure along the ab plane. Weak π–π stacking interactions are seen between the thiophene and pyridine rings, and are shown in detail in Fig. 7. The distance between the centroids of the rings is 3.8(4) Å, typical of π–π interactions.[84] The planes spanned by the rings, however, are not co-planar and intersect at an angle of 10.1°. CH⋯π interactions between oxazoline hydrogen atoms and neighbouring pyridine and thiophene rings with distances of 2.74(6) and 2.66(7) Å, respectively, are also present, as shown in Fig. 7.
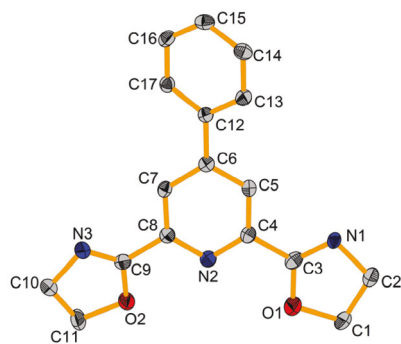

Scheme 1 Synthesis of PyboxPh **1**.

Fig. 1 Thermal ellipsoid plot of PyboxPh, **1**, with atom labelling. Hydrogen atoms were omitted for clarity. Ellipsoids at 50% probability.
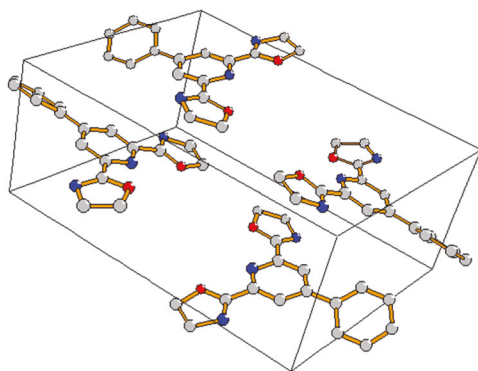

Fig. 2 Ball-and-stick diagram of the unit cell of PyboxPh **1** showing cell edges. Hydrogen atoms were omitted for clarity.
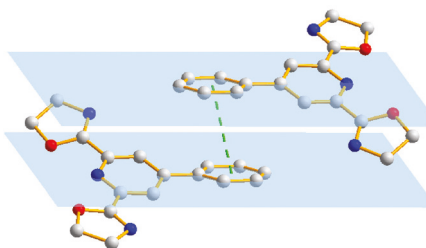

Fig. 3 Ball-and-stick diagram of PyboxPh, **1**, showing the $\pi-\pi$ stacking interaction as dashed line. The blue planes contain the phenyl rings. Hydrogen atoms were omitted for clarity.

The absorption, excitation and emission spectra of **2** are shown in Fig. 8. In acetonitrile, **2** displays an absorption maximum at 348 nm, which is at lower energy than in Pybox3Th, which absorbs at 260 nm.[86] Excitation and emission maxima at 382 and 454.5 nm, respectively, are also shifted with respect to the excitation and emission maxima of Pybox3Th, which are at 312 and 490 nm, respectively.[56] The shifts seen in the absorption, excitation and emission maxima are an indication that the presence and location of the sulfur atom of the thiophene ring play an important role in the excited state energies of the compounds.
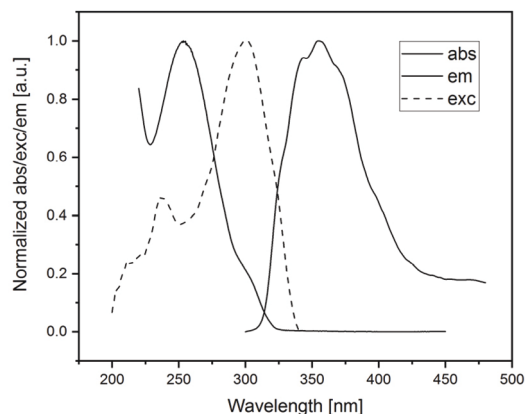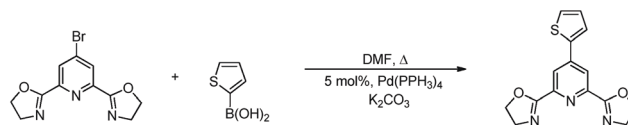

Fig. 4 Absorption (solid left), excitation (dashed) and emission (solid right) spectra of PyboxPh, **1**, in acetonitrile. λ_{em} = 355 nm, λ_{exc} = 300.5 nm. [Compound] = 1×10^{-4} M.

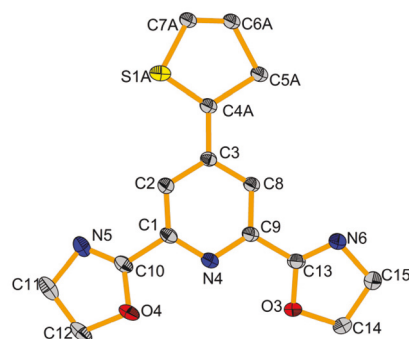**Scheme 2** Synthesis of Pybox2Th **2**.

Fig. 5 Thermal ellipsoid plot of Pybox2Th, **2**, with atom labelling. Hydrogen atoms and minor component of disordered thiophene were omitted for clarity. Ellipsoids at 50% probability.

Synthesis and characterization of [Eu(PyboxPh)(NO₃)₃H₂O] (3) and [Tb(PyboxPh)(NO₃)₃H₂O]·2H₂O (4)

Treatment of Ln[III] nitrate salts with equimolar amounts of **1** and **2** allowed us to isolate X-ray quality crystals for the 1 : 1 ligand-to-metal ion complexes of PyboxPh with Eu[III] (**3**) and Tb[III] (**4**). Crystallographic details are summarized in Table 1. The two complexes are isostructural. **3** will be discussed here representatively. It crystallizes in the triclinic $P\bar{1}$ space group, with two molecules in the unit cell. Its structure is shown in Fig. 9. The structure of **4** is shown in Fig. 10. The metal ion is coordinated to the three nitrogen atoms of the PyboxPh ligand, in addition to three bidentate nitrate anions. The coordination sphere also includes one water molecule, for a coordination number of 10, resulting in a bicapped square antiprismatic coordination geometry, shown in Fig. 11a. The
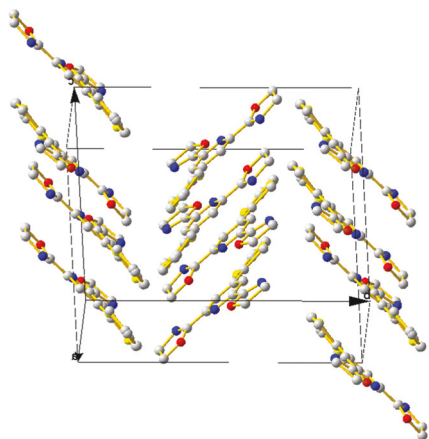
Fig. 6 Ball-and-stick diagram of the unit cell of Pybox2Th showing cell edges. Hydrogen atoms were omitted for clarity.
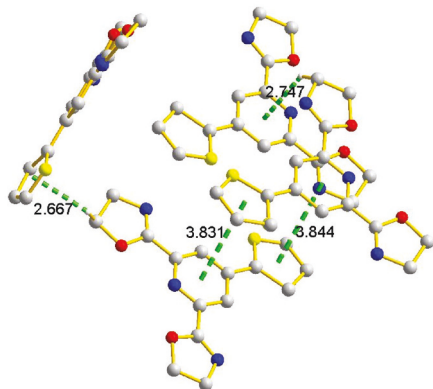

Fig. 9 Thermal ellipsoid plot of **3**, [Eu(PyboxPh)(NO$_3$)$_3$H$_2$O], with atom labeling. Hydrogen atoms were omitted for clarity. Selected bond distances [Å] are Eu1−N1 2.632(6), Eu1−N2 2.549(6), Eu1−N3 2.549(0), Eu1−O3 2.459(7), Eu1−O4 2.516(9), Eu1−O5 2.509(5), Eu−O7 2.504(5), Eu−O9 2.561(3), Eu−O10 2.457(1), Eu−O12 2.487(8).

Fig. 7 Ball-and-stick diagram representing the π−π stacking and the CH···π interactions present in Pybox2Th with relevant distances in Å. Hydrogen atoms not involved in CH···π bonding were omitted for clarity.

Fig. 10 Thermal ellipsoid plot of **4**, [Tb(PyboxPh)(NO$_3$)$_3$H$_2$O]·2H$_2$O, with atom labeling. Hydrogen atoms and disordered solvent water molecules were omitted for clarity. Selected bond distances [Å] are Tb1−N1 2.568(4), Tb1−N2 2.492(8), Tb1−N3 2.5379(8), Tb1−O3 2.416(7), Tb1−O4 2.489(8), Tb1−O5 2.586(5), Tb1−O7 2.488(4), Tb1−O8 2.497(0), Tb1−O10 2.488(7), Tb1−O11 2.511(1).
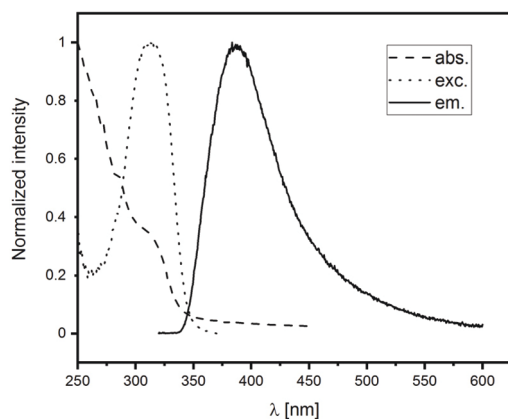

Fig. 8 Absorption (dashed), excitation (dotted) and emission (solid) spectra of Pybox2Th, **2**, in acetonitrile. λ_{em} = 388 nm, λ_{exc} = 314 nm. [Compound] = 1 × 10^{-4} M.
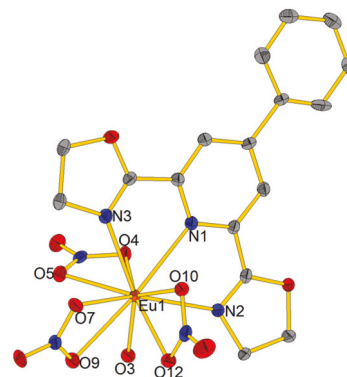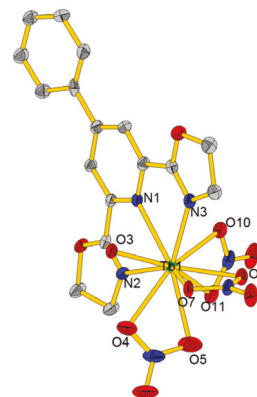

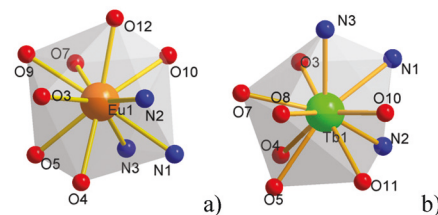**Fig. 11** Coordination polyhedra showing the bicapped square antiprismatic coordination geometry around the metal ion of (a) [Eu(PyboxPh)(NO$_3$)$_3$H$_2$O] and (b) [Tb(PyboxPh)(NO$_3$)$_3$H$_2$O]·2H$_2$O. For the Tb complex, atoms O4, O5, O11, N2 and O3, O7, O8, N1, make up the bottom and top of the square antiprism respectively while N3 and O10 are the capping atoms.

base and top of the antiprism are composed of atoms O4, O5, N1, N3 and O3, O7, O10, N2, respectively, and atoms O9 and O12 are the capping atoms. The coordination polyhedron around Tb[III] is shown in Fig. 11b. In the complexes, the torsion angle between the phenyl and pyridine rings is smaller than in the free ligand, at 2.470(5)° and 6.057(6)° for the Eu[III] and Tb[III] complexes, respectively. The Eu–N distances are in the range 2.549(3)–2.633(3) Å and the Eu–O distances are in the range 2.460(2)–2.520(3) Å, with the bond to the water molecule oxygen atom being the shortest. The Tb–N distances are in the range 2.492(8)–2.568(4) Å and the Tb–O distances are in the range 2.416(7)–2.586(5) Å with the bond to the water molecule oxygen atom again being the shortest. These distances are comparable to the distances found for other Pybox complexes of Eu[III] and Tb[III] previously described by our group.[56,87] Hydrogen bonding interactions are observed between coordinated water molecules and nitrate anions (Fig. 12).

Previous work on Pybox complexes shows that the 3 : 1 ligand-to-metal ion stoichiometry provides complete saturation of the coordination sphere of the metal ion.[56,60,87] Since crystals with this stoichiometry could not be isolated, we identified the formation of the 3 : 1 complexes by absorption titration of the ligands with the metal salts, as detailed in the Experimental section. Emission studies were performed on the 3 : 1 species with the nitrate or triflate salts in acetonitrile or dichloromethane. The emission of $[Tb(PyboxPh)_3]^{3+}$ and $[Eu(PyboxPh)_3]^{3+}$ is observed in solution and the solid state and the solution absorption, excitation and emission spectra are shown in Fig. 13. The absorption spectra of the metal complexes are equivalent to each other and are similar to the free ligand, shifted only by 13 nm for PyboxPh when coordinated to Eu[III] and 14 nm when coordinated to Tb[III]. The excitation spectra follow the absorption spectra closely, showing that emission sensitization occurs through the ligand. The emission spectra are typical of Eu[III] and Tb[III], with peaks arising

Fig. 13 Absorption (dotted black line), excitation (dashed blue line) and emission spectra of $[Eu(PyboxPh)_3]^{3+}$ (solid red line) and emission spectrum of $[Tb(PyboxPh)_3]^{3+}$ (dashed green line) measured as the triflate salts in dichloromethane and $[Ln^{III}] = 1.0 \times 10^{-4}$ M. $\lambda_{exc} = 320$ nm.

from the $^5D_0 \rightarrow {}^7F_J$ (J = 1, 2, 3, 4) transitions for Eu[III] and $^5D_4 \rightarrow {}^7F_J$ (J = 6, 5, 4, 3, 2) transitions for Tb[III].

No measurable emission was seen for the $[Tb(Pybox2Th)_3]^{3+}$ species, as will be discussed below, due to the low energy of the triplet state. However, the $[Eu(Pybox2Th)_3]^{3+}$ species was strongly emissive. Its absorption, excitation and emission spectra are shown in Fig. 14. The absorption maximum for the complex is only shifted by 1 nm with respect to the free ligand. As seen for the complexes with PyboxPh, the close resemblance between absorption and excitation spectra is supportive of ligand-based sensitization. Further, the excitation spectrum indicates that lower energy sensitization to almost 400 nm is possible, which is desirable not only from an energy efficiency point of view but also for applications involving biological media.

Determination of emission quantum yields Φ for each 3 : 1 species was performed in dichloromethane with the triflate
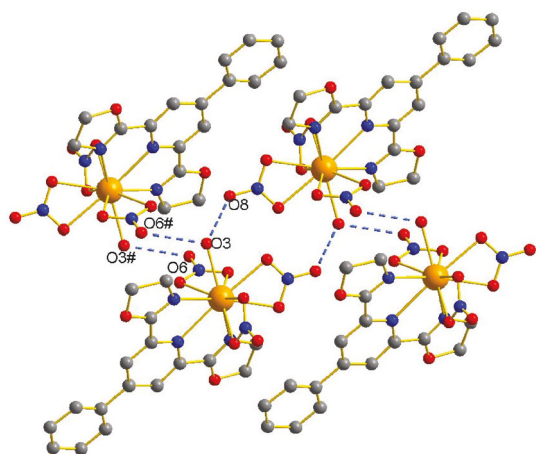

Fig. 12 Hydrogen bonding interactions between coordinated water molecules and nitrate anions for compound **3**. Distances [Å] and angles [°] are O3–O8 2.914(3), O3–O6# 2.859(4), O6#–O3–O8 108.8(1).
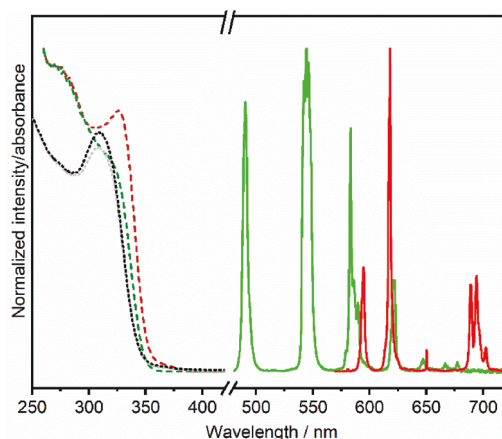

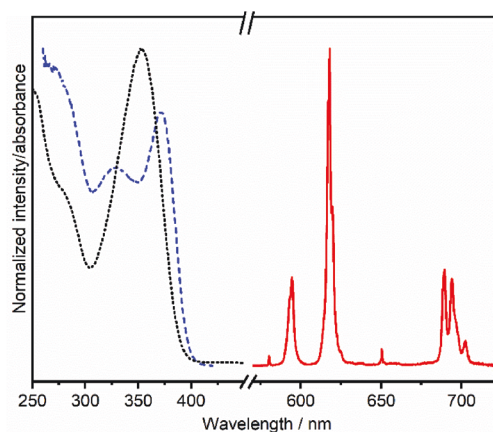**Fig. 14** Absorption (dotted black line), excitation (dashed blue line) and emission spectra of $[Eu(Pybox2Th)_3]^{3+}$ (solid red line) measured as the triflate salt in dichloromethane and $[Eu^{III}] = 1.0 \times 10^{-4}$ M. $\lambda_{exc} = 370$ nm.

Table 2 Luminescence lifetimes (τ) and quantum yields (Φ) of emission of [LnL$_3$](CF$_3$SO$_3$)$_3$ where Ln = Eu, Tb with L = PyboxPh or Pybox2Th in dichloromethane, compared with the previously reported [Ln(Pybox3Th)$_3$]$^{3+}$.[56] [Ln^{III}] = 1.0×10^{-4} M

Complex	τ [ms]	Φ [%]	ϕ_{Eu}^{Eu}	η_{sens}
[Eu(Pybox3Th)$_3$]$^{3+}$	2.097 ± 0.081	76.2 ± 6.6	—	—
[Tb(Pybox3Th)$_3$]$^{3+}$	0.367 ± 0.032	58.6 ± 4.1	—	—
[Eu(Pybox2Th)$_3$]$^{3+}$	0.714 ± 0.001	14.5 ± 0.9	21.3	68.1
[Eu(PyboxPh)$_3$]$^{3+}$	2.227 ± 0.003	37.2 ± 2.0	55.5	67.1
[Tb(PyboxPh)$_3$]$^{3+}$	0.723 ± 0.016	24.0 ± 1.3	—	—

Table 3 Singlet (^{1}S) and triplet (^{3}T) state energies of PyboxPh and Pybox2Th measured as [Gd(PyboxPh)$_3$]$^{3+}$ and [Gd(Pybox2Th)$_3$]$^{3+}$ from the nitrate salts in acetonitrile,[a] and CIS calculated (in parenthesis), compared with the energies of the previously reported Pybox3Th.[56] [Gd^{III}] = 1.0×10^{-4} M

Ligand	λ_{em} [nm]	^{1}S (calc.) [cm^{-1}]	^{3}T (calc.) [cm^{-1}]
PyboxPh	355	29 860 ± 190 (27 770)	22 250 ± 30 (22 790)
Pybox3Th		28 310 ± 310 (26 060)	21 080 ± 80 (22 500)
Pybox2Th	388	26 170 ± 230 (25 720)	19 380 ± 70 (20 210)

[a] Indicated as the 0–0 transition.

Fig. 15 Energy of ligand singlet ^{1}S and triplet ^{3}T states as a function of the functional group resonance parameter R.

salts of the Ln^{III} ions using the dipicolinate salts as standards,[78,79] as detailed in the Experimental section. The data are summarized in Table 2, along with the excited state lifetimes τ. The highest emission quantum yield was achieved for [Eu(PyboxPh)$_3$]$^{3+}$ at 37.2%; the quantum yield of [Eu(Pybox2Th)$_3$]$^{3+}$ is lower at 14.5%. Though all the triplet states of the Pybox ligands (Table 3) occur at energies which are appropriate for sensitization of Eu^{III} emission, the highest quantum yield obtained to date by a Pybox ligand was for [Eu(Pybox3Th)$_3$]$^{3+}$ with 76.2%.[56] We attribute this to an optimum matching of triplet and emissive Eu^{III} excited state as well as singlet and triplet energies. With respect to the two ligands discussed in this manuscript, despite differences in triplet state energies (Table 3), which prevent sensitization of Tb^{III} emission in the case of Pybox2Th, both ligands display similar sensitization efficiencies η_{sens} (Table 2); the differences in sensitization efficiency for Eu^{III} emission are attributed to a lower intrinsic quantum yield ϕ_{Eu}^{Eu} (Table 2) for the thienyl-bearing ligand.

In fact, when plotting the singlet and triplet state energies of the PyboxPh, Pybox2Th, and Pybox3Th ligands as a function of the resonance parameter (R)[88] of the *para* functional groups, a linear relationship is obtained, as seen in Fig. 15. Despite the small number of examples in this study, this result seems to indicate that the energy levels of the previously reported Pybox3Th are positioned just right to achieve optimum energy transfer to both Eu^{III} and Tb^{III}. Comparison with the singlet and triplet state energies of the previously reported PyboxR, where R = OMe, H, Br, also shows that the aromatic groups result in much more dramatic changes in the ligand excited
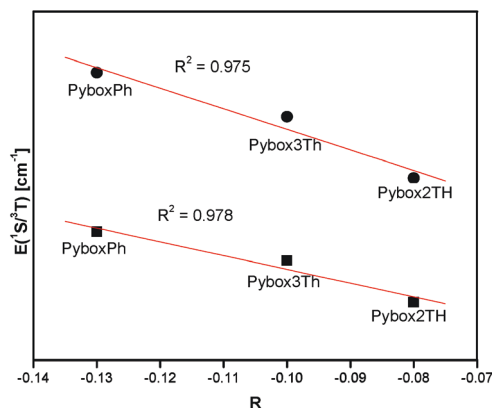
state energies than the electron-donating and withdrawing substituents.

Conclusions

Two Pybox-based antennas have been synthesized and characterized, PyboxPh and Pybox2Th. The latter expands the library of already known Pybox compounds to examples in which the *para*-substitution leads to extended π-electron systems. These two ligands readily coordinate to Ln^{III} ions. The complexation of PyobxPh with Eu^{III} and Tb^{III} led to the isolation of two new complexes, the isostructural [Eu(PyboxPh)(NO$_3$)$_3$H$_2$O] and [Tb(PyboxPh)(NO$_3$)$_3$H$_2$O]·2H$_2$O, which were characterized by single crystal X-ray diffraction. These crystals are luminescent, as are solutions of PyboxPh with Eu^{III} and Tb^{III} and Pybox2Th with Eu^{III}. The photophysical characterization of these solutions shows that the quantum yields of emission are 47.8%, 28.1%, and 40.0% respectively. The high efficiencies observed are a consequence of the appropriate position of the singlet and triplet state energies of the ligands, which are also responsible for the lack of sensitization of Tb^{III} in the case of Pybox2Th. Finally, the results presented here indicate that the singlet and triplet state energies of a Pybox-based ligand can be fine-tuned by choosing the appropriate aromatic *para* substituent. More importantly, the changes in singlet and triplet excited states with aromatic substituents are more dramatic than the ones seen for non-aromatic, electron-withdrawing or donating substituents. This opens an avenue for achieving specific singlet and triplet energy levels of the ligands through targeted ligand derivatization.

Conflicts of interest

There are no conflicts of interest to declare.

Acknowledgements

Notes and references

1 A. de Bettencourt-Dias, *Curr. Org. Chem.*, 2007, **11**, 1460–1480.

2 A. de Bettencourt-Dias, in *Luminescence of Lanthanide Ions in Coordination Compounds and Nanomaterials*, ed. A. de Bettencourt-Dias, Wiley, 2014.

3 J.-C. G. Bünzli and S. V. Eliseeva, *Springer Ser. Fluoresc.*, 2011, **7**, 1–46.

4 *Lanthanide Probes in Life, Chemical and Earth Sciences: Theory and Practice*, ed. J. C. G. Bünzli and G. R. Choppin, Elsevier, 1989.

5 A. de Bettencourt-Dias, *Dalton Trans.*, 2007, 2229–2241.

6 J.-C. G. Bünzli and C. Piguet, *Chem. Soc. Rev.*, 2005, **34**, 1048–1077.

7 F.-F. Chen, Z.-Q. Chen, Z.-Q. Bian and C.-H. Huang, *Coord. Chem. Rev.*, 2010, **254**, 991–1010.

8 G. F. de Sá, O. L. Malta, C. de Mello Donegá, A. M. Simas, R. L. Longo, P. A. Santa-Cruz and E. F. da Silva Jr., *Coord. Chem. Rev.*, 2000, **196**, 165–195.

9 C. M. G. dos Santos, A. J. Harte, S. J. Quinn and T. Gunnlaugsson, *Coord. Chem. Rev.*, 2008, **252**, 2512–2527.

10 S. V. Eliseeva and J.-C. G. Bünzli, *Chem. Soc. Rev.*, 2010, **39**, 189–227.

11 V. Bulach, F. Sguerra and M. W. Hosseini, *Coord. Chem. Rev.*, 2012, **256**, 1468–1478.

12 S. Faulkner, L. S. Natrajan, W. S. Perry and D. Sykes, *Dalton Trans.*, 2009, 3890–3899.

13 J. Andres and K. E. Borbas, *Inorg. Chem.*, 2015, **54**, 8174–8176.

14 C. Y. Chow, S. V. Eliseeva, E. R. Trivedi, T. N. Nguyen, J. W. Kampf, S. Petoud and V. L. Pecoraro, *J. Am. Chem. Soc.*, 2016, **138**, 5100–5109.

15 N. Dannenbauer, S. H. Zottnick and K. Mueller-Buschbaum, *Z. Anorg. Allg. Chem.*, 2017, **643**, 1991–1996.

16 J. D. Einkauf, J. M. Clark, A. Paulive, G. P. Tanner and D. T. de Lill, *Inorg. Chem.*, 2017, **56**, 5544–5552.

17 J.-Y. Hu, Y. Ning, Y.-S. Meng, J. Zhang, Z.-Y. Wu, S. Gao and J.-L. Zhang, *Chem. Sci.*, 2017, **8**, 2702–2709.

18 V. A. Ilichev, L. I. Blinova, A. V. Rozhkov, T. V. Balashova, R. V. Rumyantcev, G. K. Fukin and M. N. Bochkarev, *J. Mol. Struct.*, 2017, **1148**, 201–205.

19 D. Kovacs, X. Lu, L. S. Meszaros, M. Ott, J. Andres and K. E. Borbas, *J. Am. Chem. Soc.*, 2017, **139**, 5756–5767.

20 E. G. Leach, J. R. Shady, A. C. Boyden, A.-l. Emig, A. T. Henry, E. K. Connor, R. J. Staples, S. Schaertel, E. J. Werner and S. M. Biros, *Dalton Trans.*, 2017, **46**, 15458–15469.

21 A. F. Martins, S. V. Eliseeva, H. F. Carvalho, J. M. C. Teixeira, C. T. B. Paula, P. Hermann, C. Platas-Iglesias, S. Petoud, E. Toth and C. F. G. C. Geraldes, *Chem. – Eur. J.*, 2014, **20**, 14834–14845.

22 M. Pan, B.-B. Du, Y.-X. Zhu, M.-Q. Yue, Z.-W. Wei and C.-Y. Su, *Chem. – Eur. J.*, 2016, **22**, 2440–2451.

23 K. Senthil Kumar, B. Schafer, S. Lebedkin, L. Karmazin, M. M. Kappes and M. Ruben, *Dalton Trans.*, 2015, **44**, 15611–15619.

24 P. J. Wright, J. L. Kolanowski, W. K. Filipek, Z. Lim, E. G. Moore, S. Stagni, E. J. New and M. Massi, *Eur. J. Inorg. Chem.*, 2017, **2017**, 5260–5270.

25 R. Xiong, J. Andres, K. Scheffler and K. E. Borbas, *Dalton Trans.*, 2015, **44**, 2541–2553.

26 S. H. Zottnick, J. A. P. Sprenger, M. Finze and K. Mueller-Buschbaum, *Eur. J. Inorg. Chem.*, 2017, **2017**, 1355–1363.

27 Y.-J. Wang, D.-F. Wu, J. Gou, Y.-Y. Duan, L. Li, H.-H. Chen, H.-L. Gao and J.-Z. Cui, *Dalton Trans.*, 2020, **49**, 2850–2861.

28 Y.-Y. Li, N. Ren, S.-M. He, S.-P. Wang and J.-J. Zhang, *Appl. Organomet. Chem.*, 2020, **34**, e5418.

29 R.-f. Li, R.-h. Li, X.-f. Liu, X.-h. Chang and X. Feng, *RSC Adv.*, 2020, **10**, 6192–6199.

30 R.-f. Li, R.-h. Li, X.-f. Liu, X.-h. Chang and X. Feng, *RSC Adv.*, 2020, **10**, 8539.

31 M. A. Hernandez-Rodriguez, C. D. S. Brites, G. Antorrena, R. Pinol, R. Cases, L. Perez-Garcia, M. Rodrigues, J. A. Plaza, N. Torras, I. Diez, A. Millan and L. D. Carlos, *Adv. Opt. Mater.*, 2020, **8**, 2000312.

32 C. Herlan and S. Braese, *Dalton Trans.*, 2020, **49**, 2397–2402.

33 H.-Y. Wong, W.-S. Lo, K.-H. Yim and G.-L. Law, *Chem*, 2019, **5**, 3058–3095.

34 J.-M. Li, R. Huo, X. Li and H.-L. Sun, *Inorg. Chem.*, 2019, **58**, 9855–9865.

35 M. Kumar, L.-H. Wu, M. Kariem, A. Franconetti, H. N. Sheikh, S.-J. Liu, S. C. Sahoo and A. Frontera, *Inorg. Chem.*, 2019, **58**, 7760–7774.

36 J.-H. Jia, Q.-W. Li, Y.-C. Chen, J.-L. Liu and M.-L. Tong, *Coord. Chem. Rev.*, 2019, **378**, 365–381.

37 D. A. Galico, R. Marin, G. Brunet, D. Errulat, E. Hemmer, F. A. Sigoli, J. O. Moilanen and M. Murugesu, *Chem. – Eur. J.*, 2019, **25**, 14625–14637.

38 A. de Bettencourt Dias and S. Viswanathan, *Chem. Commun.*, 2004, 1024–1025.

39 A. de Bettencourt-Dias, *Inorg. Chem.*, 2005, **44**, 2734–2741.

40 S. Viswanathan and A. de Bettencourt-Dias, *Inorg. Chem. Commun.*, 2006, **9**, 444–448.

41 S. Viswanathan and A. de Bettencourt-Dias, *Inorg. Chem.*, 2006, **45**, 10138–10146.

42 A. de Bettencourt-Dias and S. Viswanathan, *Dalton Trans.*, 2006, 4093–4103.

43 A. de Bettencourt-Dias, S. Bauer, S. Viswanathan, B. C. Maull and A. M. Ako, *Dalton Trans.*, 2012, **41**, 11212–11218.

44 A. de Bettencourt-Dias and P. S. Barber, *C. R. Chim.*, 2010, **13**, 691–699.

45 A. de Bettencourt-Dias and J. S. K. Rossini, *Inorg. Chem.*, 2016, **55**, 9954–9963.

46 R. A. Tigaa, G. J. Lucas and A. de Bettencourt-Dias, *Inorg. Chem.*, 2017, **56**, 3260–3268.

47 J. H. S. K. Monteiro, F. A. Sigoli and A. de Bettencourt-Dias, *Can. J. Chem.*, 2018, **96**, 859–864.

48 R. A. Tigaa, X. Aerken, A. Fuchs and A. de Bettencourt-Dias, *Eur. J. Inorg. Chem.*, 2017, 5310–5317, DOI: 10.1002/ejic.201700655.

49 J. H. S. K. Monteiro, D. Machado, L. M. de Hollanda, M. Lancellotti, F. A. Sigoli and A. de Bettencourt-Dias, *Chem. Commun.*, 2017, **53**, 11818–11821.

50 J. H. S. K. Monteiro, D. Machado, L. M. de Hollanda, M. Lancellotti, F. A. Sigoli and A. de Bettencourt-Dias, *Chem. Commun.*, 2017, **53**, 11818–11821.

51 J. H. S. K. Monteiro, A. de Bettencourt-Dias, I. O. Mazali and F. A. Sigoli, *New J. Chem.*, 2015, **39**, 1883–1891.

52 K. R. Johnson and A. de Bettencourt Dias, *Inorg. Chim. Acta*, 2021, **514**, 120003.

53 G. Desimoni, G. Faita and P. Quadrelli, *Chem. Rev.*, 2003, **103**, 3119–3154.

54 G. Desimoni, G. Faita, M. Guala and A. Laurenti, *Eur. J. Org. Chem.*, 2004, 3057–3062.

55 H. C. Aspinall, *Chem. Rev.*, 2002, **102**, 1807–1850.

56 A. de Bettencourt-Dias, S. Viswanathan and A. Rollett, *J. Am. Chem. Soc.*, 2007, **129**, 15436–15437.

57 A. de Bettencourt-Dias and P. S. Barber, *C. R. Chim.*, 2010, **13**, 691–699.

58 A. de Bettencourt-Dias, P. S. Barber and S. Bauer, *J. Am. Chem. Soc.*, 2012, **134**, 6987–6994.

59 J. Yuasa, T. Ohno, K. Miyata, H. Tsumatori, Y. Hasegawa and T. Kawai, *J. Am. Chem. Soc.*, 2011, **133**, 9892–9902.

60 A. de Bettencourt-Dias, P. S. Barber, S. Viswanathan, D. T. de Lill, A. Rollett, G. Ling and S. Altun, *Inorg. Chem.*, 2010, **49**, 8848–8861.

61 M. Andrews, A. J. Amoroso, L. P. Harding and S. J. A. Pope, *Dalton Trans.*, 2010, **39**, 3407–3411.

62 S. Sivakumar, M. L. P. Reddy, A. H. Cowley and K. V. Vasudevan, *Dalton Trans.*, 2010, **39**, 776–786.

63 C. Kachi-Terajima, K. Yanagi, T. Kaziki, T. Kitazawa and M. Hasegawa, *Dalton Trans.*, 2011, **40**, 2249–2256.

64 N. M. Shavaleev, R. Scopelliti, F. Gumy and J.-C. G. Bünzli, *Inorg. Chem.*, 2009, **48**, 6178–6191.

65 M. Pan, X.-L. Zheng, Y. Liu, W.-S. Liu and C.-Y. Su, *Dalton Trans.*, 2009, 2157–2169, DOI: 10.1039/B818322H.

66 A. Beeby, L. M. Bushby, D. Maffeo and J. A. Gareth Williams, *J. Chem. Soc., Dalton Trans.*, 2002, 48–54.

67 C. S. Bonnet, F. Buron, F. Caillé, C. M. Shade, B. Drahoš, L. Pellegatti, J. Zhang, S. Villette, L. Helm, C. Pichon, F. Suzenet, S. Petoud and É. Tóth, *Chem. – Eur. J.*, 2012, **18**, 1419–1431.

68 E. S. Andreiadis, R. Demadrille, D. Imbert, J. Pécaut and M. Mazzanti, *Chem. – Eur. J.*, 2009, **15**, 9458–9476.

69 E. S. Andreiadis, R. Demadrille, D. Imbert, J. Pécaut and M. Mazzanti, *Chem. – Eur. J.*, 2009, **15**, 9458–9476.

70 Q. Wang, K. Tang, X. Jin, X. Huang, W. Liu, X. Yao and Y. Tang, *Dalton Trans.*, 2012, **41**, 3431–3438.

71 S. Petoud, J.-C. G. Bünzli, K. J. Schenk and C. Piguet, *Inorg. Chem.*, 1997, **36**, 1345–1353.

72 X. Yu, T. Yang, S. Wang, H. Xu and H. Gong, *Org. Lett.*, 2011, **13**, 2138–2141.

73 A. I. Vogel, *Elementary Practical Organic Chemistry. Pt. 3. Quantitative Organic Analysis*, Longmans, Green & Co., 1958.

74 SMART, *Bruker Molecular Analysis Research Tool, v5.626*, Bruker AXS, Madison, WI, 2002.

75 SAINTPlus, *DATA Reduction and Correction Program, v.6.36a*, Bruker AXS, Madison, WI, 2001.

76 SADABS, *An empirical absorption correction program, V.2.01*, Bruker AXS, Madison, WI, 2001.

77 G. M. Sheldrick, *SHELXTL, Structure Determination Software Suite, v.6.10*, Bruker AXS, Madison, WI, 2001.

78 A.-S. Chauvin, F. Gumy, D. Imbert and J.-C. G. Bünzli, *Spectrosc. Lett.*, 2004, **37**, 517–532.

79 A.-S. Chauvin, F. Gumy, D. Imbert and J.-C. G. Bünzli, *Spectrosc. Lett.*, 2007, **40**, 193.

80 M. H. V. Werts, R. T. F. Jukes and J. W. Verhoeven, *Phys. Chem. Chem. Phys.*, 2002, **4**, 1542–1548.

81 J. D. L. Dutra, T. D. Bispo and R. O. Freire, *J. Comput. Chem.*, 2014, **35**, 772–775.

82 MOPAC2012, J. J. P. Stewart, *Stewart Computational Chemistry*, 2012.

83 F. Neese, *Wiley Interdiscip. Rev.: Comput. Mol. Sci.*, 2012, **2**, 73–78.

84 M. Nishio, M. Hirota and Y. Umezawa, *CH/π Interaction: Evidence, Nature, and Consequences*, Wiley-VCH, 1998.

85 *Disorder and Strain-Induced Complexity in Functional Materials*, ed. T. Kakeshita, T. Fukuda, A. Saxena and A. Planes, [*In: Springer Ser. Mater. Sci.*, 2012; 148], Springer, 2012.

86 A. de Bettencourt-Dias, S. Viswanathan and A. Rollett, *J. Am. Chem. Soc.*, 2007, **129**, 15436–15437.

87 A. de Bettencourt-Dias, P. S. Barber and S. Bauer, *J. Am. Chem. Soc.*, 2012, **134**, 6987–6994.

88 C. Hansch, A. Leo and R. W. Taft, *Chem. Rev.*, 1991, **91**, 165–195.